Asymmetric fission of ^{236}U in a self-consistent K-matrix model*

D. Kolb†
Yale University, New Haven, Connecticut 06520

R. Y. Cusson‡
Duke University, Durham, North Carolina 27706

H. W. Schmitt§
Oak Ridge National Laboratory, Oak Ridge, Tennessee 37830

(Received 25 February 1974; revised manuscript received 6 June 1974)

The phenomenological single-particle Hamiltonian of Meldner is rederived as a renormalized single-particle K matrix and is used to calculate the properties of ^{236}U on the fission path from the ground state to scission into asymmetric fragments. Substantial radial density fluctuations or "bubble configurations" are observed as well as a displacement of the neutron center of mass relative to that of the protons. It is also found that the presence of a deep minimum and saddle near the touching point can be observed for one of the parameter sets of the interaction. The parameters of our deformation and atomic number independent model were obtained by fitting to the experimental properties of ^{16}O, ^{40}Ca, ^{48}Ca, and ^{208}Pb and nuclear matter. The present results illustrate the importance of using a nonorthogonal two-oscillator basis as well as taking into account the properties of nuclear matter.

[NUCLEAR STRUCTURE, FISSION ^{236}U; calculated fission path, shape asymmetry, static total energy, single particle energies. Self-consistent Brueckner-Hartree-Fock method.]

I. INTRODUCTION

The recent successes[1-3] of the liquid drop formulas combined with the single-particle shell model (Nilsson model, two-center model, deformed Woods-Saxon model, etc.) via a Strutinsky renormalization has stimulated renewed interest in more fundamental models which would combine both liquid drop and shell-model effects in one single energy operator. In such a model, the nuclear shape, the total energy, as well as the single-particle properties should not, if possible, be predetermined but be computed in a self-consistent iterative scheme. This paper uses such a model, based ultimately on the Brueckner-Hartree-Fock theory of nuclei, and applies it to the calculation of the fission of ^{236}U.

Among the various attempts at a basic calculation of nuclear fission, the simplest is the Hartree-Fock (HF) model with an effective two-body potential. This method suggests itself from its successes in atomic and molecular physics, yet it does not work too well in nuclear fission problems because it neglects important short-range rearrangement effects due to the strong repulsive core of the nucleon-nucleon interaction. Attempts to incorporate the effects of the hard core in a HF treatment have been made by either using an effective three-body interaction of the Skyrme type[4] or by considering explicitly density dependent effective interactions and reaction matrices.[5] Although the reaction matrix approach is the most fundamental, it is also the most complex. Thus the present paper simplifies this approach by using a semiphenomenological single-particle K-matrix model.[6,7] This effective deformed shell-model Hamiltonian is used to compute the potential energy surface near the minimum energy fission path in a self-consistent manner. The model was first applied to spherical nuclei,[6] where most of its parameters are determined. It was next shown[7] to provide a good representation for the light deformed nuclei although *all* of the model parameters are determined either from nuclear matter or for spherical magic nuclei. Many important further refinements are of course possible, but the importance of the heavy nucleus fission problem is such that one should quickly establish whether or not these models can yield reasonable representations of the fission energy curve. As we shall see in this work, it appears that this approach is quite capable of yielding total energy curves which include *both* the liquid drop *and* the shell correction energy. Some uncertainties in the results have been found, but as we shall see, they can be traced to the uncertainties in the nuclear matter properties used to obtain the model parameters.

Section II outlines the basic features of the mod-

el in nuclear matter. There appears the rearrangement term so essential to the approach, as an additional term in the single-particle Hamiltonian. A particularly simple special case[6] is singled out and is used in this work because of its ease of handling and of previous experience[6,7] with it. Section III deals with the application of the model to finite nuclei. In particular, attention is paid to the Coulomb interaction,[7-9] the isospin properties, the spin-orbit splitting, and the kinetic energy of the center of mass. There, one also discusses the density formalism used to make the transition from nuclear matter to finite nuclei, along with such questions as the pairing algorithm and the application of constraints.

Section IV covers important practical matters such as the Gaussian fractionated expansion[7-9] and the values of the model parameters and gives estimates for the optimum values of the number of shells and oscillator parameters in the one- and two-oscillator bases used in this work. Finally, that section discusses the matter of the initialization of the density and the iterative procedure used to obtain the self-consistent density at each point on the fission curve.

Section V shows the results for the structure of the potential energy curve of ^{236}U, and the corresponding self-consistent densities on the fission path. In particular we stress some of the predicted density fluctuation properties which, in places, show up as incipient bubble structures. The displacement of the neutron-proton centers of mass in the fragments is noted along with bulk octupole deformation, the asymmetric mass distribution, and the early influence of the fragment shells in determining the mass asymmetry ratio. The similarities and differences with molecular clusters are also discussed before concluding.

II. RENORMALIZED K MATRIX IN NUCLEAR MATTER

We shall begin with a model[6-8] for the antisymmetrized, momentum conserving nuclear matter matrix elements of the Brueckner two-body reaction matrix $\langle k_1, k_2 \mid K(k_0) \mid k_1, k_2 \rangle$, in the Fermi gas model representation. We consider those matrix elements of the form $K(k_1, k_2, k_0)$, where k_0 is the Fermi momentum related to the total density ρ_0 by

$$k_0^3 = \tfrac{3}{2}\pi^2 \rho_0 , \tag{2.1}$$

and k_1 and k_2 denote the momenta of particles 1 and 2. One next postulates a separable expansion of the form

$$K(k_1, k_2, k_0) = \sum_{\alpha\beta} G_{\alpha\beta}(k_0) f_\alpha(k_1) f_\beta(k_2), \tag{2.2}$$

where, to be more precise, the dependence on k_0 should be replaced by a functional dependence on the state occupation function $\rho(k) = n(k)$ for spin and isospin saturated nuclear matter. The complex dependence of $G_{\alpha\beta}$ on $n(k)$ may be approximated to first order in $n(k)$ by

$$G_{\alpha\beta}[n] = \int_0^\infty k^2 dk \; \bar{g}_{\alpha\beta}(k) n(k) + g^0_{\alpha\beta} , \tag{2.3}$$

so that if $n(k) = 1$ up to k_0, and 0 after that, we get

$$G_{\alpha\beta}[n] = \int_0^{k_0} k^2 dk \; \bar{g}_{\alpha\beta}(k) + g^0_{\alpha\beta} = G_{\alpha\beta}(k_0) . \tag{2.4}$$

The total energy of A particles in a box of volume Ω becomes

$$W = \sum_i (\hbar^2/2m) k_i^2 n_i + \frac{1}{2} \sum_{ij} n_i n_j (\pi^2/2\Omega) K(k_i, k_j, [n]) . \tag{2.5}$$

This equation will be used later to compute the total energy and right away to obtain, after some algebra, the single-particle energy

$$\epsilon(k, k_0) = \frac{\delta W}{\delta n_k} = \frac{\hbar^2}{2m} k^2 + \sum_{\alpha\beta} G_{\alpha\beta}(k_0) f_\alpha(k) F_\beta(k_0) + \frac{1}{2} \sum_{\alpha\beta} \bar{g}_{\alpha\beta}(k) F_\alpha(k_0) F_\beta(k_0) , \tag{2.6}$$

where

$$F_\alpha(k_0) = \int_0^\infty k^2 dk \; f_\alpha(k) n(k) \cong \int_0^{k_0} k^2 dk \; f_\alpha(k) . \tag{2.7}$$

The last term of Eq. (2.6) is the Brueckner rearrangement potential, which is now dependent on *both* k and k_0. Unfortunately, the details of the momentum dependence of $\Delta(k)$ are not well known, although there is increasing evidence that one cannot simultaneously obtain the correct nuclear matter compressibility and the correct shell model level density from a local (momentum independent) Δ. However, we shall follow, in this paper, the current practice[5-7] and consider only models where $\bar{g}_{\alpha\beta}(k) = \bar{g}_{\alpha\beta}(k_0)$, e.g., where Δ is local. This simplifying assumption is believed to be mainly responsible for the fact, here as in most calculations of this kind, that although the overall level density is correct, the level density in the neighborhood of the Fermi sea is too small by some 35%. The model[6] discussed in the following sections further simplifies the isospin dependence of the potential (see Sec. III). It keeps,

however, the essential feature of being a finite range potential, thus extending its validity beyond ground states to excited nuclear configurations as occurring in nuclear fission and heavy ion scattering (fusion). Another benefit of a finite range potential is the insensitivity of gross structures against parameter variations (see Sec. V). The special restrictions of Meldner's[6] model need of course not be imposed on Eq. (2.6) and they have already been successfully lifted.[8] A study of such more sophisticated models for deformed and fissioning configurations is in progress.

Returning to Eq. (2.6) we now continue our development by picking an explicit model to represent that rearranged energy. We follow Meldner[6] and set

$$\epsilon(k, k_0) = \hbar^2 k^2/2m - \tfrac{1}{2} V_0[v(k)\bar{u}(k_0) + \bar{u}(k_0)v(k)] + \Delta(k_0) \tag{2.8}$$

as the simplest possible one-term separable representation of the single-particle reaction matrix $\epsilon(k, k_0)$ (so-called because it includes the energy due to the Brueckner rearrangement reaction), where $\Delta(k_0)$ is the Brueckner rearrangement potential at $k = k_0$; we also use

$$v(k) = \frac{1}{1 + (ak)^2}, \tag{2.9}$$

$$\bar{u}(k_0) = \left(\frac{k_0}{k_e}\right)^3 \frac{[1 - (k_0/k_1)^{3\gamma}]}{[1 - (k_e/k_1)^{3\gamma}]}, \tag{2.10}$$

so that $\bar{u}(k_e) = 1$, where k_e is the nuclear matter equilibrium Fermi momentum. These forms lead to the expression for Δ as

$$\Delta(k_0) = \tfrac{1}{2} V_0 \left[v(k_0)\bar{u}(k_0) - F_0(k_0) \frac{1}{k_0^2} \frac{\partial \bar{u}(k_0)}{\partial k_0} \right], \tag{2.11}$$

where

$$F_0(k_0) = \int_0^{k_0} k^2 dk\, v(k). \tag{2.12}$$

The parameters V_0, k_1, and a are determined by choosing the nuclear matter equilibrium momentum k_e, the binding energy per nucleon at equilibrium, and $\Delta(k_0)$ the Brueckner rearrangement energy (at the Fermi momentum k_0). The two values $\gamma = \frac{2}{3}$ and $\gamma = 1$ were used and changed little else except the nuclear compressibility $\kappa = k_0^2 \partial^2 E_b(k_0)/\partial k_0^2$. Finally the Yukawa kernel $v(k)$ was approximated to sufficient accuracy by a three-term Gaussian superposition[9] in the range $0 \leq k \leq 1.5 k_0$.

III. FINITE NUCLEI

The transition to finite nuclei is made in the spirit of an energy density functional approach. Thus, one can consider the total energy per unit volume, with a volume element centered at $\vec{r}$ inside the nucleus, then one differentiates with respect to the density at $\vec{r}$ to obtain the single-particle energy density $\epsilon(k, k_0(r))$. Other corrections due to the inhomogeneity of the nucleus and to isospin and spin-orbit effects must also be made. Lastly, the all-important Coulomb interaction must be treated with great care.

A. Isospin, spin-orbit, and inhomogeneity corrections

Whereas the extreme simplicity of the present model precludes an exact treatment of the isospin properties, we simply follow the earlier prescription[6] obtained from physical arguments. Thus we set

$$k_0^\tau = [3\pi^2 \rho_\tau]^{1/3}, \quad \begin{matrix} \tau = 1 \text{ protons} \\ \tau = -1 \text{ neutrons}, \end{matrix} \tag{3.1}$$

and we define the effective density $\tilde{\rho}_\tau$ for particles of kind τ as

$$\tilde{\rho}_\tau = (\tau_0 \rho_\tau + \rho_{-\tau})/(1 + \tau_0), \tag{3.2}$$

where τ_0 is a dimensionless parameter of order 0.4; ρ_τ is the true density of protons and neutrons

$$\rho_\tau(r) = \sum_\lambda n_\lambda^\tau |\phi_\lambda(r)|^2, \tag{3.3}$$

with n_λ^τ the number of particles of kind τ in orbit λ, and $\phi_\lambda(r)$ the single-particle wave function of orbit λ. The function $\bar{u}(k_0)$ defines a function $u(\rho) = \bar{u}(k_0)$. Thus the functions $u(\tilde{\rho}_\tau)$ were used throughout. The expression for Δ in the isospin formalism is more elaborate and was derived as[7]

$$\Delta(\vec{k}_0^\tau) = \tfrac{1}{2} V_0 \left\{ v(k_0^\tau) u(\tilde{\rho}_\tau) - \left[F_0(k_0^\tau) \frac{\partial u(\tilde{\rho}_\tau)}{\partial \tilde{\rho}_\tau} \tau_0 + F_0(k_0^{-\tau}) \frac{\partial u(\tilde{\rho}_{-\tau})}{\partial \tilde{\rho}_{-\tau}} \right] \Big/ [(1 + \tau_0)\pi^2] \right\}. \tag{3.4}$$

The spin-orbit potential is introduced in its semiempirical form[7,10]

$$v_{\vec{l}\cdot\vec{s}}^\tau = \tfrac{1}{2} C[v(k)\vec{\sigma} \cdot (\vec{\nabla} u_\tau \times \vec{k})] + \text{H.c.} \tag{3.5}$$

One notes that this form is quite appropriate for nuclear fission as $v_{\vec{l}\cdot\vec{s}}$ goes over, in the fragmentation limit, to the correct spin-orbit potentials of the fragments; this is due mainly to the fact that u is almost linear in ρ, the constant k_1 in Eq. (2.10) being large.

The inhomogeneity corrections can be performed by using a suitable spacial average of the density in our density functional approach. Thus we replace ρ_τ by

$$\bar{\rho}_\tau(r)=\frac{1}{[(4\pi)^{3/2}\xi^3]}\int d^3r'\,\rho_\tau(r')e^{-|r-r'|^2/4\xi^2} \tag{3.6}$$

in the construction of the single-particle Hamiltonian. The averaging length ξ is of order 0.5 fm. This corresponds to having a r.m.s. radius of 1.22 fm for the folding form factor in Eq. (3.6). This should be a reasonable estimate of the correlation distance in single-particle states of the nucleus.

The self-consistent method to be followed is now becoming clear. One picks an initial guess for $\rho_p(r)$ and $\rho_n(r)$. This allows one to construct $\epsilon^\tau(k,r)=h^\tau(k,r)$, the single-particle Hamiltonian, as a function of momentum and position. One then diagonalizes h:

$$h^\tau(k,r)\phi_\lambda(r)=\epsilon^\tau_\lambda\phi(r). \tag{3.7}$$

The eigenvalues ϵ^τ_λ are used in a BCS type formalism to construct the occupation number n^τ_λ of the state ϕ_λ for the next iteration. Then one uses Eq. (3.3) to construct the new density. This iteration is repeated until no further changes in $\rho^\tau(r)$ are observed [usually 10 to 25 iterations will suffice, depending on the accuracy of the initial guess for $\rho(r)$]. This algorithm will, of course, lead to a stable minimum in the energy-configuration space. When one wants to obtain some other point on the fission curve, one must impose constraints. They will be discussed in the next section.

B. Coulomb potential

The Coulomb potential consists of two terms, the exchange term v_{CE} and the direct term $v_{CD}(r)$ which is given by

$$v_{CD}(r)=\int d^3r'\,\frac{\rho_p(r')}{|r-r'|}. \tag{3.8}$$

The first step in obtaining v_{CD} is to expand the Coulomb kernel as a sum of Gaussians of varying range[9] and strengths. We shall see in Sec. IV that $\rho_p(r)$ is also expanded in Gaussians along the Z and r cylindrical coordinates; this allows one to perform the integral exactly and to obtain $v_{CD}(r)$ again as a superposition of Gaussian terms with an accuracy of one part in 10^4 up to a radius of about 25 fm.

The exchange term v_{CE} was computed using a statistical approximation[7,9]

$$v_{CE}\cong\begin{cases}\dfrac{-5}{4Z}\left[\dfrac{3}{2\pi Z}\right]^{2/3}E_{CD} & \text{for occupied states},\\ 0 & \text{for unoccupied levels},\end{cases} \tag{3.9}$$

where E_{CD} is the total direct Coulomb energy. Again we have verified that this expression will provide a good approximation up to the scission (touching) point, which is as far as we have gone in this work.

C. Center-of-mass kinetic energy correction

The operator for the kinetic energy with respect to the center of mass can be readily obtained as

$$T_{rel}=\sum_{i=1}^{A}(p_i^2/2m)(1-1/A)-(1/2mA)\sum_{i\neq j}\vec{p}_i\cdot\vec{p}_j. \tag{3.10}$$

The second part of this expression is a two-body operator whose direct term vanishes, on the average, due to the *fixed* position of the center of mass. The average one-body exchange part of Eq. (3.10) may be estimated again in the statistical, or free Fermi gas, model to be

$$t_E(\lambda)=\begin{cases}\dfrac{\langle\lambda|p^2|\lambda\rangle}{MA} & \lambda \text{ an occupied state},\\ 0 & \lambda \text{ a free state}.\end{cases} \tag{3.11}$$

This last expression is particularly interesting in that it predicts a vanishing value for the total kinetic energy of the center of mass. Thus essentially similar results would have been obtained by completely *neglecting* the kinetic energy of the center of mass. Previous calculations[7] on ^{8}Be have in fact confirmed that no major spurious center-of-mass excitations seem to arise from the present combined treatment of the kinetic energy and of the momentum dependent potential energy.

D. Constraints

As pointed out earlier, the simple iterative process where h is repeatedly diagonalized, using successive improvements for the density $\rho(r)$, leads to a configuration which is a local minimum in the total energy surface. Since our aim is to trace out the minimum energy path to fission, we must provide some external field interaction (constraint) which will make one of the nonminimal configurations a temporary minimum in the presence of the constraint field. The constraints are introduced by assuming that the total energy Eq. (2.11) should be modified by the external field in-

teraction H_I; e.g.,

$$W_{\text{net}} = W + H_I, \quad H_I = \tfrac{1}{2}\lambda(M_0 - M)^2, \tag{3.12}$$

where M stands for a multipole moment operator, M_0 for that value of the operator at which the interaction energy vanishes, and λ is the strength of the external interaction. It can be seen that for sufficiently large λ, any energy minimization principle which uses W_{net} instead of W will tend to favor configurations for which $\langle M\rangle \cong M_0$, since it is those configurations which have the smaller values for W_{net}. If we now vary W_{net} with respect to n_k, we obtain[7] after some algebra

$$h_{\text{net}} = h + \lambda(M_0 - \langle M\rangle)M, \tag{3.13}$$

where $\langle M\rangle$ is the current expectation value of M. We have used Eq. (3.13) with $M = Q_2^0$, the mass quadrupole operator. The normalization constant can be picked by demanding that for a 20% deviation of $\langle M\rangle$ from M_0, the net quadrupole energy be about the *same* as that for the appropriate deformed oscillator having $\hbar\omega = 41/A^{1/3}$.

This type of constraint is suitable for most configurations along the fission path whose greatest difference from stationary configurations is in the *quadrupole* moment value. For configurations whose *higher multipole moments* are also changing rapidly, Eq. (3.13) can exhibit substantial instabilities. These instabilities are such that in order to obtain the *desired values* of M_3 and M_4, one must clamp M_2 *very* tightly (λ large). However, large values of λ lead to undesired oscillations in the energy and unwanted changes in the density distributions. One could, of course, use $H_I = \sum_k \frac{1}{2}\lambda_k(M_0^k - M^k)^2$, but one would have to pick precise and correlated values of M_0^k; however, these correlated values are just the information we are *seeking* from the calculation. There is in fact a much easier way to provide scissioning type constraints, which is connected with the choice of the two-oscillator basis. One simply selects the centers of the two oscillators to be sufficiently far apart that the edges of the basis (the semiclassical turning points coordinates) trace out connected regions in space with some necking in. As we shall see in the next section the lack of orthogonality of the eigenfunctions of such oscillators poses no difficulties. We shall also see there that as long as the corresponding necking in the *momentum space* is small enough not to come down to momentum values of occupied states, the total energy is not *directly* affected by this constraint whereas the coordinate dependence of $\rho(r)$ is biased heavily towards necked, or in the extreme limit clustered, configurations. This is just what is needed to compute the total energy past the second minimum and towards binary scission while injecting the minimum bias via the constraints. This method is, of course, similar to the one used in atomic and molecular physics where it is called the molecular orbitals technique. The only added complication here is the fission instability of those molecular configurations.

E. Pairing corrections

The pairing energy corrections play a very important role insofar as they are closely connected with the essential question of determining the occupation numbers of the orbits from a knowledge of the values of the single-particle energies. The more basic approach to the pairing question consists in selecting the pairing energy functional $W_p(n_i)$ to be added to the total energy expression (2.5). In the case of finite nuclei one then varies W_{tot} with respect to $\phi_i(\vec{r})$ *and* n_i, where $\rho(r) = \sum_i |\phi_0|^2 n_i$, subject to the number conservation constraint $n = \sum_i n_i$. These yield equations of the BCS type for n_i. Whereas the BCS formalism can lead to sophisticated convergence difficulties in a large basis we have chosen to dampen the pairing interaction by using a state dependent gap parameter $\Delta_p(\epsilon_i)$ as

$$\Delta_p(\epsilon_i) = \Delta_0 \exp\{-[(\epsilon_i - \lambda)/D_0]^2\}, \tag{3.14}$$

with

$$\Delta_0 \cong 15\ \text{MeV}/\sqrt{A}, \quad D_0 \cong 15\ \text{MeV}/A^{1/3}, \tag{3.15}$$

and λ the Fermi energy, from which the occupation numbers n_i can be determined in the usual BCS fashion.[3] The atomic number dependence of Δ_0 is a little stronger than the usual $12/\sqrt{A}$ because of our somewhat low level density at the Fermi sea. The value of D_0 is in rough agreement with the energy half-width of the more realistic pairing matrix elements $\langle k, -k | V(r - r') | k, -k\rangle$, and was actually determined by the requirement that the occupation number of states which are $\hbar\omega$ in energy above the Fermi sea be less than 10^{-4}. The expression (3.14) automatically removes the pairing correction for spherical nuclei and makes the whole procedure insensitive to the size of the basis as long as it is greater than one major shell above and below the Fermi sea, a requirement easily met by the present calculation.

Finally one should mention that our present assumption of zero nuclear temperature gives the absolute ground state energy surface. However, as one goes past the second barrier one cannot be sure that none of the fission energy goes into thermal modes of excitation.[1,3] Finite temperature pairing calculations are relatively easy to perform and will be reported elsewhere.

IV. SELECTED ASPECTS OF THE CALCULATION

We will discuss here only the most important of the various practical matters connected with a calculation of the present magnitude. First we discuss the oscillator basis structure and the companion Gaussian expansion technique. Then the influence of the parameter set on the calculation will be studied and finally the important matter of selecting the initial density will be brought up.

A. Gaussian expansion

We shall work in a basis consisting of the nonorthogonal eigenstates of two shifted, deformed, axially symmetric harmonic oscillators. In such a basis it was found convenient to expand the single-particle density of Eq. (3.3), as well as other density dependent functions, in sums of axially symmetric Gaussian terms[7,9]

$$f(\boldsymbol{r}) = \sum_{\nu,\mu}^{n,m} a_{\nu\mu} \exp\left[-\lambda_\nu R^2 - \beta_\mu (Z - Z_\mu)^2\right], \qquad (4.1)$$

where R is the cylindrical coordinate $(X^2+Y^2)^{1/2}$ and $a_{\nu\mu}$, λ_μ, and β_μ are coefficients to be determined by a nonlinear fitting procedure. For configurations near the ground state Z_μ is usually taken to be zero, but for strongly clustered states, where the two-oscillator features are essential to insure reasonable convergence of the basis, three different values of Z_μ were used, namely

$$\begin{aligned} Z_1 &= \text{center of oscillator 1}, \\ Z_3 &= (Z_1 b_2^2 - Z_2 b_1^2)/(b_1^2 + b_2^2), \\ Z_2 &= \text{center of oscillator 2}, \end{aligned} \qquad (4.2)$$

where b_1 and b_2 are the Z-direction oscillator parameters of the basis. The limit $m \cong 7$ was used for each three values of Z_μ in the fitting procedure. The choice of these three shift points for the Gaussians is, of course, natural since these are the centers of the oscillator Gaussians for the components of $\rho(\boldsymbol{r})$ in oscillator 1, in the 1×2 interference part, and in oscillator 2; e.g.,

$$\rho(\boldsymbol{r}) = \rho_1(\vec{\mathbf{r}}, Z_1) + \rho_3(\vec{\mathbf{r}}, Z_3) + \rho_2(\vec{\mathbf{r}}, Z_2) \qquad (4.3)$$

arises naturally from the expansion (3.3). Other functions of $\rho(\boldsymbol{r})$ are easily fragmented as

$$f(\rho(\vec{\mathbf{r}})) = \sum_{i=1}^{3} f_i(\vec{\mathbf{r}}), \quad f_i(\vec{\mathbf{r}}) = \frac{f(\rho(\vec{\mathbf{r}}))\,\rho_i(\vec{\mathbf{r}})}{\rho(\vec{\mathbf{r}})}. \qquad (4.4)$$

This last equation is, of course, useful whenever one wishes to expand clustered functions with nonzero overlap. Again, attempts to fit strongly clustered f's without fractionating usually demand so many terms in the expansion that great numerical convergence difficulties are encountered in the determination of the λ's and the β's. But in any case it would be less economical to use a method centered at $Z=0$ in dealing with strongly clustered functions. Thus, the present fractionating techniques should also be useful in schemes where the matrix elements are obtained by direct numerical integration methods[8] such as Gauss-Laguerre or Gauss-Hermite schemes.

B. Basis selection

Two different bases have been used in this calculation: for relatively small deformations a one-oscillator, orthogonal, axially symmetric basis was used in cylindrical coordinates; for large deformations and clustered states another similar but shifted oscillator was added. In both cases the number of basis states for the $k=\frac{1}{2}$ Hamiltonian matrix was restricted to 72.

When using deformed oscillators one must be sure to select the states to be included *not* according to their major shell quantum numbers, but rather according to their harmonic oscillator energies $\hbar\omega_z(n_z+\frac{1}{2})+\hbar\omega_\perp(n_\perp+1)$. By equipartition of energy this means we must include all states up to a given cutoff *kinetic* energy. This, of course, reflects the fact that nuclei which are deformed in coordinate space actually remain very nearly spherical in *momentum* space; e.g., their Fermi surface is almost a sphere even in extreme cases such as the scission point.

It is possible to derive equations relating the values of N the major shell quantum number and b the oscillator parameter to be used in the calculation of a nucleus. Here we shall consider a spherical nucleus but the argument is easily extended to deformed ones. To begin with we note that $\rho(r, k)$, the density matrix which gives the density of particles at the point (r, k) in the phase space of a spherical nucleus, is approximately given as

$$\rho(r,k) \cong \begin{cases} 4/(2\pi)^3, & 0 \le r \le R_{1/2}, \quad 0 \le k \le k_0, \\ 0 \text{ otherwise}. \end{cases} \qquad (4.5)$$

This defines a square in the two dimensional plane of the variables $x = r/R_{1/2}$ and $y = k/k_0$. Now a spherical harmonic oscillator with maximum major shell quantum number N_m and oscillator parameter b covers, at uniform density, the region of phase space inside the ellipse

$$y^2(bk_0)^2 + x^2\left(\frac{R_{1/2}}{b}\right)^2 = 2(N_m + \tfrac{3}{2}). \qquad (4.6)$$

The ellipse with the smallest value of N which does *not* cut off the corner $x=1, y=1$ of the density distribution, is a *circle* with *radius* $R_h = \sqrt{2}$. The

circular condition gives

$$bk_0 = R_{1/2}/b\,, \qquad b = (R_{1/2}/k_0)^{1/2}\,. \tag{4.7}$$

The other equation gives

$$(N_m + \tfrac{3}{2}) = R_h^2\, \tfrac{1}{2} R_{1/2} k_0\,. \tag{4.8}$$

We note that the minimal model which can in any way represent the nucleus is the one where one completely fills the oscillator basis and one chooses $R_h = 1$. In that case Eqs. (4.7) and (4.8) give the familiar Nilsson model rules for choosing the oscillator parameter. For our present purpose we must use $R_h \gtrsim \sqrt{2}$. Using the values $R_h = \sqrt{2}$, $R_{1/2} = 7$ fm, $k_0 \cong 1.35$ fm^{-1}, appropriate for ^{208}Pb, gives $\hbar\omega = 8$ MeV, $N_m \cong 8$ which is approximately $2\,\hbar\omega$ higher than the Fermi sea. As seen previously by Flocard, $N_m = 12$ is actually necessary for good convergence in ^{208}Pb; this corresponds to $R_h \cong 1.7$ and indicates that one must also provide for a good fit to the tail of the wave function both in coordinate space and in momentum space.

Quite similar considerations have been made and used in the case of a single deformed oscillator except that the phase space envelopes are now four dimensional for axial symmetry. In the case of the two-oscillator basis the analysis can become quite complex because one must study the intersection of four-dimensional surfaces. The following prescription has been used: we keep each oscillator spherical (except around scission on the fission path where both fragments are highly stretched), selecting their oscillator parameters according to the desired size of the region through Eq. (4.7). We shift the oscillators until the neck radius of the envelopes defined by the semiclassical turning point $R_{1/2}$ comes within ~2 fm of the actual nuclear surface. This prescription proved to be quite close to the optimum basis. As mentioned earlier, this method also had the advantage of readily providing a smooth necking constraint.

C. Model parameters

The model used in the present calculation allows variation in its parameters as a means of absorbing into the parametrization the inaccuracies implied by the approximations used. Table I gives three typical sets of such parameters, while Table II gives single-particle energies for sets I and III; we now discuss the properties and merits of these sets.

To begin with we point out that the spin-orbit parameter is fixed mainly by the experimental spin-orbit splitting in heavy nuclei. Changing C within a reasonable range only has minor effects on the energy surface; thus the value given in the table was used throughout. Similarly, the isospin parameter τ_0 should be varied only in a relatively small range about the value which makes the neutron-proton force approximately 2 to 3 times stronger than the neutron-neutron or proton-proton force. The value of τ_0 also influences the symmetry energy and the relative depth of the neutron and proton Fermi energies. These depths are reasonable with the values chosen; however, the nuclear matter symmetry energy was not computed as the highly phenomenological isospin dependence of our model makes the extrapolation to nuclear matter of dubious interest.

The inhomogeneity correction parameter ξ was determined by demanding optimum values for the radii and binding energy of ^{40}Ca and ^{208}Pb while remaining in a physical region for its value. We note that the r.m.s. radius of the averaging form factor in Eq. (3.6) is $\sqrt{6}\,\xi$. Thus the values of ξ shown in Table I correspond to a smearing radius of about 1.1 fm. This is consistent with the range of the nuclear force. When ξ is too *small* the calculated nuclear radii decrease and the binding energies increase. These effects are reversed for large ξ.

The remaining nuclear matter parameters V_0, ρ_1, and a are mainly determined by the required nuclear matter properties k_e, E_b, $\partial E_b/\partial k_e = 0$, $\Delta(k = k_0)$. The final determination of the parameters V_0, ρ_1, and a was done together with an adjustment of C, ξ, and τ_0 (Table I) from the binding energies, radii, and single-particle spectra of ^{16}O, ^{40}Ca, ^{48}Ca, and ^{208}Pb as given in Tables II and III. The then corresponding nuclear matter parameters are also displayed in Table I.

TABLE I. Parameter sets used in the calculation: V_0, E_b, $\Delta(k_0)$, κ in MeV, a, ξ in fm, k_0 in fm^{-1}, ρ in nucleons/fm^3, C in MeV fm^2, γ and τ_0 are dimensionless.

Parameter set	V_0	a	ρ_1	2ξ	C	τ_0	E_b	$\Delta(k_0)$	γ	κ	k_0
I	96.49	0.5124	0.2476	0.913	23.5	0.45	15.95	13.0	3	303	1.333
II	107.97	0.6932	0.3190	0.878	23.5	0.4	15.6	8.0	2	213	1.31
III	108.73	0.6966	0.2584	0.913	23.5	0.4	15.75	8.0	3	261	1.31

TABLE II. Single-particle energies for sets I and III: $\epsilon'^{(1)}$ energies are defined by Eq. (2.8), $\epsilon'^{(3)}$ follow by the replacement $v(k) \rightarrow \frac{1}{2}[v(k)+v(k_0)]$. (See Ref. 7.) These energies are negative unless otherwise indicated. For experimental results, see Ref. 4.

		Neutrons			Protons		
		I $\epsilon'^{(1)}$	III $\epsilon'^{(3)}$	Exp	I $\epsilon'^{(1)}$	III $\epsilon'^{(3)}$	Exp
^{16}O	$1s_{1/2}$	46.1	51.9		42.4	48.3	40±8
	$1p_{3/2}$	24.1	25.0	21.8	20.8	21.8	18.4
	$1p_{1/2}$	16.7	18.4	15.7	13.3	15.1	12.1
	$1d_{5/2}$	7.2	6.1	4.14	3.6	2.5	0.6
	$2s_{1/2}$	2.0	1.7	3.27	+1.7	+1.9	0.1
^{40}Ca	$1s_{1/2}$	59.7	69.2		51.7	61.4	50±11
	$1p_{3/2}$	42.5	46.5		35.0	39.2	34±6
	$1p_{1/2}$	38.0	42.3		30.4	34.9	
	$1d_{5/2}$	25.6	26.1		18.6	19.3	
	$2s_{1/2}$	18.2	19.3	18.1	11.0	12.3	10.9
	$1d_{3/2}$	18.0	19.5	15.6	10.8	12.5	8.3
	$1f_{7/2}$	10.7	9.5	8.36	3.5	2.4	1.4
	$2p_{3/2}$	4.2	3.9	6.2			
^{48}Ca	$1s_{1/2}$	60.3	69.1		55.4	65.8	55±9
	$1p_{3/2}$	44.3	48.1		40.1	45.3	35±7
	$1p_{1/2}$	40.6	44.7		36.4	41.9	
	$1d_{5/2}$	28.3	28.8		24.5	26.1	
	$2s_{1/2}$	21.1	22.9	12.55	16.7	18.6	15.3
	$1d_{3/2}$	21.5	22.1	12.52	17.6	20.1	15.7
	$1f_{7/2}$	12.9	11.6	9.94	9.5	9.0	9.6
	$2p_{3/2}$	6.6	6.36	5.14	1.8	2.1	1.9
	$2p_{1/2}$	4.2	4.23	3.11	0.2	+0.1	0.0
	$1f_{5/2}$	4.7	5.03			1.3	

^{208}Pb

	Neutrons					Protons				
	I		III			I		III		
	$\epsilon'^{(1)}$	$\epsilon'^{(3)}$	$\epsilon'^{(1)}$	$\epsilon'^{(3)}$	Exp	$\epsilon'^{(1)}$	$\epsilon'^{(3)}$	$\epsilon'^{(1)}$	$\epsilon'^{(3)}$	Exp
$1s_{1/2}$	68.8	43.8	81.4	42.9		55.3	33.3	68.7	33.0	
$1p_{3/2}$	61.0	40.5	70.4	39.6		48.1	30.5	60.0	30.4	
$1p_{1/2}$	60.3	39.7	69.7	38.8		47.2	29.6	57.1	29.4	
$1d_{5/2}$	52.3	36.4	58.7	35.5		39.7	26.9	46.4	26.7	
$1d_{3/2}$	50.6	34.6	57.1	33.9		37.7	24.8	44.5	24.8	
$2s_{1/2}$	48.0	33.4	54.0	32.7		34.4	23.0	40.6	23.2	
$1f_{7/2}$	42.9	31.6	46.8	30.8		30.5	22.4	34.4	22.3	
$1f_{5/2}$	39.9	28.5	44.1	28.0		27.1	19.0	31.3	19.2	
$2p_{3/2}$	36.7	27.1	40.1	26.6		23.2	17.1	26.5	17.4	
$2p_{1/2}$	35.4	25.9	39.0	25.5		21.8	15.8	25.3	16.1	
$1g_{9/2}$	33.1	26.1	35.0	25.3		20.9	17.2	22.5	17.1	15.43
$1g_{7/2}$	28.6	21.6	31.1	21.4		15.9	12.2	18.1	12.8	11.43
$2d_{5/2}$	25.4	30.3	27.1	20.0		12.2	10.4	13.5	10.8	9.7
$2d_{3/2}$	23.2	18.2	25.2	18.1		9.8	8.2	11.4	8.9	9.37
$1h_{11/2}$	23.0	19.9	23.3	19.1		10.9	11.1	10.9	10.9	8.38
$3s_{1/2}$	22.4	17.9	24.2	17.8		8.7	7.5	10.2	8.2	8.03
$1h_{9/2}$	16.9	13.9	18.3	14.1	10.85	3.8	4.1	4.7	5.0	3.77
$2f_{7/2}$	14.6	13.0	15.1	12.9	9.72	1.0	2.5	1.1	3.1	2.87
$1i_{13/2}$	12.9	13.1	12.2	12.2	9.01	0.5	3.8	+0.8	3.6	2.16
$3p_{3/2}$	11.1	10.0	11.7	10.2	8.27	+3.0	+0.9	+2.2	+0.06	0.95
$2f_{5/2}$	11.6	10.1	12.6	10.4	7.95	+2.3	+0.5	+1.7	0.5	0.47
$3p_{1/2}$	9.9	8.9	10.6	9.2	7.38					
$2g_{9/2}$	4.7	5.7	4.6	5.7	3.94					
$1i_{11/12}$	5.6	5.9	6.3	6.4	3.05					

TABLE II. (*Continued*)

	Neutrons					Protons				
	I		III			I		III		
	$\epsilon'^{(1)}$	$\epsilon'^{(3)}$	$\epsilon'^{(1)}$	$\epsilon'^{(3)}$	Exp	$\epsilon'^{(1)}$	$\epsilon'^{(3)}$	$\epsilon'^{(1)}$	$\epsilon'^{(3)}$	Exp
$1j_{15/2}$	3.2	5.7	1.7	5.1	2.53					
$3d_{5/2}$	1.4	2.7	1.4	3.0	2.36					
$4s_{1/2}$	0.02	1.3	0.04	1.8	1.91					
$2g_{7/2}$	1.1	2.2	1.5	2.8	1.45					
$3d_{3/2}$	+0.3	1.0	+0.08	1.6	1.42					

Set I is distinguished by its higher values of k_e and $\Delta(k_e)$; this leads directly to higher values of κ (the compressibility) and seems to be responsible for the fact that this set gave a considerably higher first barrier than the other sets, as can be seen in Table III which shows some bulk parameters for the three sets. Set II has lower values of κ and lower values of the first barrier but its use of the exponent $\gamma = 2$ makes it somewhat less realistic in the context of a momentum dependent $\Delta(k)$. The low value of κ is related to the higher radii obtained with this set. The increased radii were partly due to a greater reaction to the repulsive Coulomb force. This set was not pursued further here. Set III was the one used to produce most of the results discussed and will be compared further to set I before we proceed. The binding energy systematics of set I is better, the radius of ^{208}Pb and ^{236}U ground state is better, but the radii of light nuclei are somewhat poorer than with set III. The higher values of κ and $\Delta(k_0)$ might suggest that set I is less realistic in the nuclear matter limit but one has to keep in mind that these values are renormalized nuclear matter values as a consequence of a momentum independent rearrangement term Δ. Again we emphasize that these arguments are not compelling since the precise details of the charge density distribution require such corrections as the inclusion of the neutron halo contribution (via the neutron form factor[11]) to the charge form factor; this correction is not applied here. Rather, we prefer to view the differences between the two sets and their results as an indication of the sensitivity on the parametrization in the present model and we found that the results for the fusion curve were quite similar except near the touching point. Finally, Fig. 1 shows density distributions for several nuclei.

D. Construction of the initial density

The rate at which the iterations will converge to the shape which is stationary in the presence of the

TABLE III. Some bulk properties for the three parameter sets. Binding energy BE in MeV, charge radius r_c in fm, the β deformation parameters defined by

$$\langle r_k^2\rangle = (\langle r_x^2\rangle\langle r_y^2\rangle\langle r_z^2\rangle)^{1/3}\exp\left[(5/\pi)^{1/2}\beta\cos\left(\tfrac{2}{3}\pi k\right)\right] \quad (k = 1, 2, 3).$$

	^{16}O	^{40}Ca	^{48}Ca	^{208}Pb	^{236}U	^{236}U*	^{236}U*
				Set I			
BE	126.4	343.2	415.6	1623.3	1789.0	1777.0	1781.5
r_c	2.65	3.40	3.50	5.56	5.87	6.04	6.13
β	0.0	0.0	0.0	0.0	0.222	0.391	0.48
				Set II			
BE	134.6	358.2	424.8	1646.9	1811.1	1802.7	1805.2
r_c	2.7	3.46	3.56	5.69	5.99	6.15	6.25
β	0.0	0.0	0.0	0.0	0.213	0.392	0.472
				Set III			
BE	129.1	348.4	412.3	1620.7	1787.3	1778.5	1779.8
r_c	2.69	3.44	3.55	5.66	5.93	6.11	6.18
β	0.0	0.0	0.0	0.0	0.185	0.389	0.451

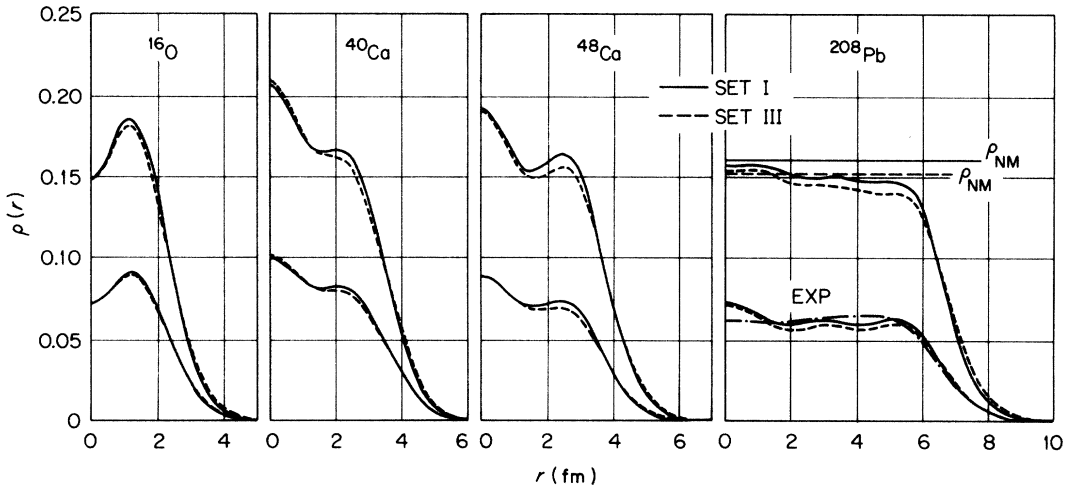

FIG. 1. Density distributions in nucleons/fm^3 vs the radius in fm for ^{16}O, ^{40}Ca, ^{48}Ca, and ^{208}Pb. The pairs with central densities near 0.15 nucleons/fm^3 represent the mass distribution while the pairs with central densities near 0.07 nucleons/fm^3 show the calculated charge density. The electron scattering experimental charge density for ^{208}Pb is also shown for comparison. Table III contains other properties of these nuclei.

constraints depends strongly on the chosen initial density. This dependence is further enhanced by the relatively high compressibility of the model which makes the total energy fairly sensitive to gross errors in the density. Two types of initial densities were used depending on the position on the fission curve. The Nilsson model was used for configurations treated with the one-oscillator basis; e.g., near the ground state and second minimum. For two-oscillator configurations a direct density construction scheme was followed. The Nilsson model was a standard deformed oscillator model with (pseudo) $\vec{l}\cdot\vec{\sigma}$ and $l^2-\langle l^2\rangle$ terms in cylindrical coordinates. This model is naturally symmetric so it was perturbed by adding to its density small asymmetric terms in order to allow the iterations the option of proceeding in the asymmetric direction. This is because of the well-known fact that self-consistent calculations usually conserve all the symmetries present in the initial

TABLE IV. Summary of properties along the fission path for set III. r_p is the r.m.s. radius of protons in fm, the multipole moments Q_l are defined as dimensionless relative quantities by

$$Q_l=\left(\frac{2^l}{(2l-1)!!}\right)^{1/2}\frac{r^l}{r_{\rm rms}^l}P_l(\cos\theta)\frac{1}{N},$$

where $P_l(x)$ are Legendre polynomials, and N is the particle number of kind τ. r_n and $Q_{l,n}$ are for neutrons, $E_{\rm Ct}$ is the total Coulomb energy in MeV, $E_{\rm pair}$ is the pairing energy in MeV, and Δz is the approximate distance in fm between the centers of the two clusters.

	Ground state	$\beta=0.33$	Second minimum	Second barrier	$\beta=0.86$	$\beta=1.025$	Scission
r_p	5.88	6.00	6.11	6.57	7.04	7.70	8.59
$Q_{2,p}$	0.138	0.25	0.372	0.530	0.665	0.758	0.816
$Q_{3,p}$	0.0	0.0	0.003	0.031	0.03	0.147	0.147
$Q_{4,p}$	0.0267	0.058	0.0401	0.0957	0.148	0.220	0.215
r_n	6.00	6.10	6.15	6.61	7.08	7.75	8.61
$Q_{2,n}$	0.137	0.235	0.346	0.510	0.635	0.740	0.802
$Q_{3,n}$	0.0	0.0	0.003	0.028	0.03	0.146	0.145
$Q_{4,n}$	0.0264	0.053	0.0311	0.0869	0.134	0.212	0.210
$E_{\rm Ct}$	935	928	923	888	823	770	728
$E_{\rm pair}$	3.4	4.8	3.5	4.5	4.96	3.7	4.1
Δz	≃3.5	≃4.7	≃5.5	≃7.5	10	12	14
r_c	5.93	6.05	6.16	6.62	7.10	7.75	8.63
Fig. Nos.	3(a), 3(b)		4(a), 4(b)	5(a), 5(b)	6	7(a), 7(b)	8(a), 8(b)

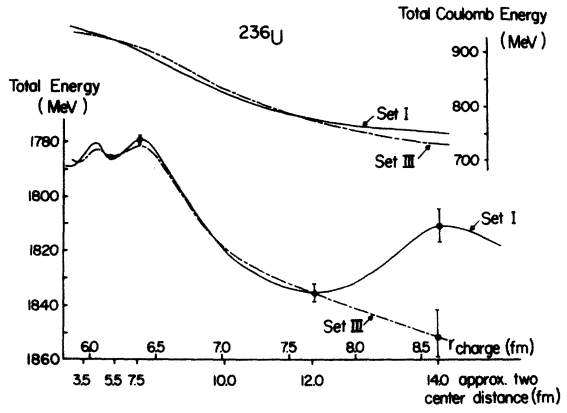

FIG. 2. Coulomb and total energies of ^{236}U as a function of the charge radius along the path to fission, using parameter set III and parameter set I. Other properties of the configurations are given in Table IV, such as multipole moments and deformation parameter β. Actual contour drawings of the proton and neutron density distributions are given in Figs. 3–9.

trial density.

The direct density construction scheme, which was used in the two-oscillator mode, first assumed a zeroth order density with a sharp surface located at $R(Z)$, $R=(x^2+y^2)^{1/2}$, and given by

$$[R(Z)/C]^2=[1-x+x(Z/D-Z_0)^\beta][1-(Z/D)^2], \tag{4.9}$$

where D, C, x, β, and Z_0 are parameters of the shape. For $x=0$ we have ellipses whose volume and deformation parameters determine C and D. When $x>0$, it is a measure of the fractional incursion of the neck while Z_0 ($-1\leq Z_0\leq+1$) gives the position of the neck and therefore controls the amount of asymmetry. The exponent β defines the neck shape and the value $\beta=1.5$ was found satisfactory in most cases.[1] The initial density distribution defined by Eq. (4.9) was next folded numerically with an approximate Gaussian form factor in order to obtain a 10–90% surface thickness of about 1.2 fm. Thus Eq. (4.9) then becomes the approxi-

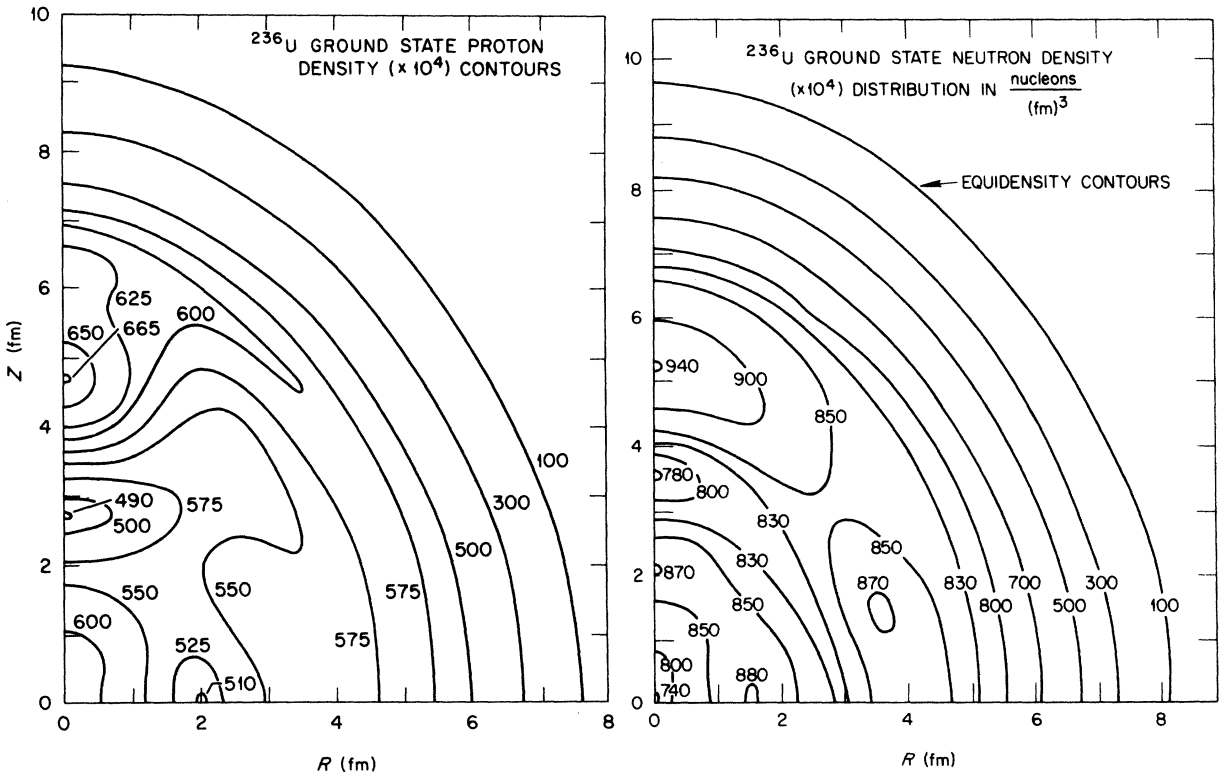

FIG. 3. (a) Equidensity contour lines for the protons in the ground state of ^{236}U. This figure, as all the others shown here, is obtained using parameter set III. The density values shown on the contours are $\rho(r)\times10^4$, $\rho(r)$ in nucleons/fm^3. Only one quadrant of the $[Z, R=(x^2+y^2)^{1/2}]$ plane is shown since the density is axially symmetric about the Z axis and reflection symmetric under the inversion $Z\rightarrow -Z$. (b) Equidensity contour lines for the neutrons in the ground state of ^{236}U. Otherwise same as (a).

mate equation for the half-density point. It was verified that the final results were insensitive to small changes in the initial density. Of course, large changes in ρ did produce completely independent excited fission configurations which are not reported here.

V. RESULTS AND DISCUSSION

Although we shall present detailed results mostly for parameter set III, we again emphasize that set I also gave reasonable results. In particular the results for the clustering effects, the single-particle energies, and the total energies as well as the total density distributions are quite similar for both sets. (See Fig. 1.) The density distributions for set I (not shown here), for example, reveal that this set yields a slightly smaller surface thickness and 5% higher maximum central density than set III. These differences do not appear to be large enough to greatly affect the properties near the ground state. However, the differences may lead to as much as a 10% change in the ratio of surface to volume energy and a 5% change in the Coulomb energy. These changes can be critical past the second barrier and going towards the touching point, as we shall see.

Table IV summarizes the properties of our ^{236}U self-consistent configurations. In particular, one of the variables which characterizes the path is the charge radius of the system $r_c \cong (r_p^2 + 0.65)^{1/2}$ where r_p^2 is the mean proton point particle radius squared. The Coulomb energies given in Table IV are used in Fig. 2 in a plot of E_c vs the charge ra-

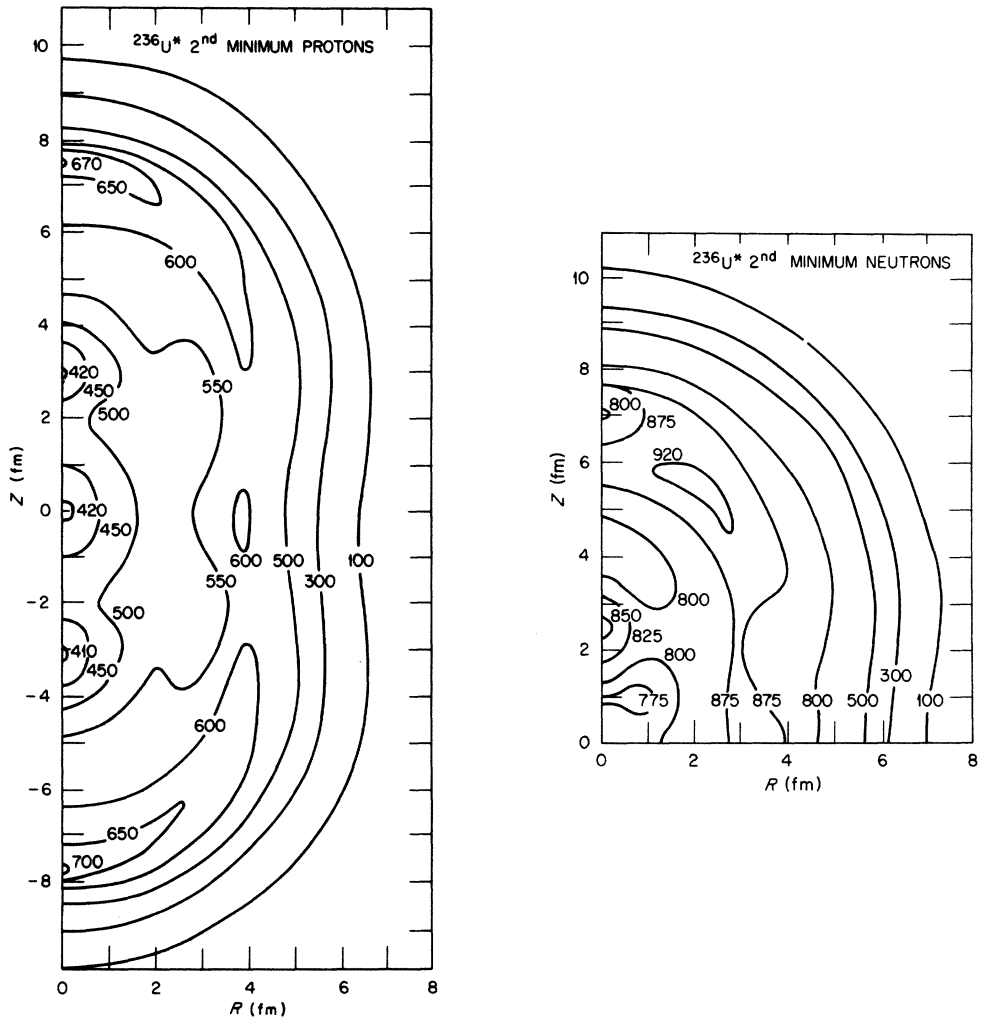

FIG. 4. (a) Proton density contours at the second minimum. One notes a small asymmetry and some "squaring off" of the density distribution. The ring at $Z=0$, $R \sim 4$ fm is still present at the second minimum, and considerable density fluctuations continue to mark the central density contours. (b) Neutron density contours at the second minimum. Only the portion with $Z \gtrsim 0$ is shown because the asymmetry is quite small. See caption to (a).

dius. The total binding energy is also given. As can be seen for set III the binding energy curve appears to be smooth from the second barrier to the touching point. This is by no means a requirement of the model. Indeed a similar calculation done with parameter set I, while giving similar results up to the second barrier, yielded the values $E_b = 1835$ MeV at $r_c = 7.7$ fm and $E_b = 1811$ MeV at $r_c = 8.6$ fm. Thus set I would allow for the existence of a quasimolecular cluster configuration having roughly the shape shown in Fig. 7(a) for $r_c \simeq 7.7$ fm. Of course, one would need to study the dynamics in order to obtain the lifetime. One problem connected with Fig. 2 should be pointed out, namely that there exist at least two minimum energy paths (fission path, fusion path) coinciding around the second barrier and further in, but separated by a barrier outside (no internal excitation and adiabaticity assumed). Except around scission (touching point respectively) the density shapes do not allow an immediate classification of belonging to a fission or fusion type configuration. Thus Fig. 6 may belong to either type. As compared with Fig. 8 which is the touching configuration on the fusion path, Fig. 7 represents a fusion type configuration also. A further exploration of the fission path involving highly deformed fragments (ratios of long axis to short axis of the order of 2) will be reported elsewhere.

The Figs. 3 to 9 show equidensity contours for the neutron and proton density distribution of ^{236}U on the fission path. These will now be discussed. Perhaps the most remarkable feature of those figures is the apparent fact that the binary cluster structure which will be finalized at scission is to a certain extent already apparent even in the ground state, when one looks at the density contours in the range 400–900. Thus, as proposed by Newson,[12] it appears that the fragment shell structure competes from the very beginning with the liquid drop properties, in determining the asymmetric nature of the present fissioning nucleus.

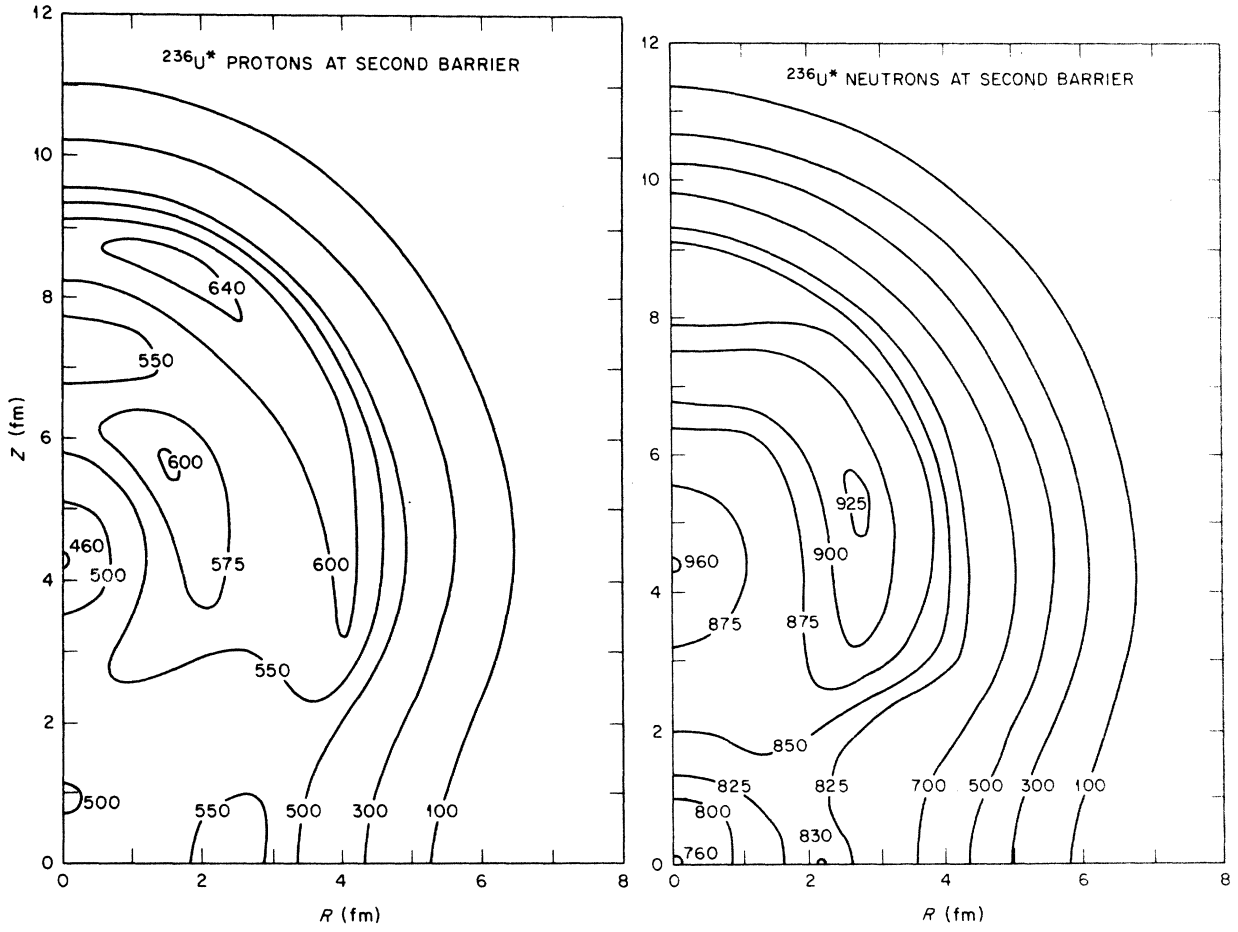

FIG. 5. (a) Proton density contours near the second barrier. Because the asymmetry is still small only the $Z \gtrsim 0$ portion is shown. (b) Neutron density contour near the second barrier.

In order to avoid discussing what may turn out to be only fluctuations, one should look at structures which are present when the total density is being considered. One of those structures is the ring in the $Z=0$ plane, with radius $R=(x^2+y^2)^{1/2}\cong 4$ fm, which can be seen in the ground state. This ring is present for most configurations and its radius begins to shrink as the system starts necking in. The ring then moves along the Z axis towards one or the other fragment, thereby breaking the symmetry of the system. The presence of density clusters is, of course, a well known property of the density distribution of light nuclei;[7,13] their presence has been proposed recently in the heavy nucleus ^{176}Yb, in order to fit electron scattering data.[14] The presence and motion of the ^{236}U ring found here also plays an important role in determining the value of the charge hexadecapole moment[15]; it also may indicate the experimental fact that prompt α particles are emitted perpendicular to the direction of motion of the binary fragments.

Continuing with our discussion we observe that Figs. 7 and 8 suggest that the mass asymmetry of the fragments is a shell effect. Namely, matter moves up in order to form a stable spherical configuration near that of the doubly magic nucleus ^{132}Sn while the remainder forms a deformation-soft ^{90}Zr-type configuration. These observations fit well with Newson's model[12] where one starts with the unperturbed single-particle spectrum of two spherical fragments with mass 132 and 78, respectively, and one builds up, by the use of statistical arguments, the fission yield curve as a function of the mass ratio, for various excitation energies of the system.

Another topic of considerable interest concerns the probable excitation modes of the fragments as they emerge from the fission process. Although we have always occupied the levels in a manner consistent with no "thermal" internal excitations, we may still expect that close inspection of the density distributions can reveal which type of excitations will be predominant. For example, excitations which are many-body correlations at the beginning of the fission process will not appear thermally at that stage but will only be converted to statistical equilibrium at some later stage. On the minimum energy fusion path the fragments observed here have masses 139 and 97, respectively (which is close to the known mass asymmetry of fissioning ^{236}U), and are not in their ground states, for most of the figures presented here. In particular, a small shift in the position of the proton vs neutron center of mass has been observed. It is a result of the Coulomb repulsion and amounts to about 0.05 fm; it sets in as soon as asymmetry begins; e.g., somewhere between the second minimum and the second barrier. In addition to this $T=1$ dipole excitation, a sizeable amount of octupole polarization can be observed in the light fragment. A third type of excitation appears in the form of radial density fluctuations or "bubble structures." Thus, the light fragment has a central depression of nearly 20% in its total density by the time one approaches scission. The heavy fragment has only a 6% depression, the smaller value possibly being due to the greater stability of the spherical configuration adopted by that fragment. These fluctuations do not appear to be very short lived either since they are basically already present at the second minimum as a 20% variation in density over the "flat" part of the central density. Indeed, it has been speculated that these fluctuations may even be stable (present in the ground state) in some Hg isotopes. A study of these isotopes in the present model is therefore indicated and will be reported elsewhere.[16] We would like

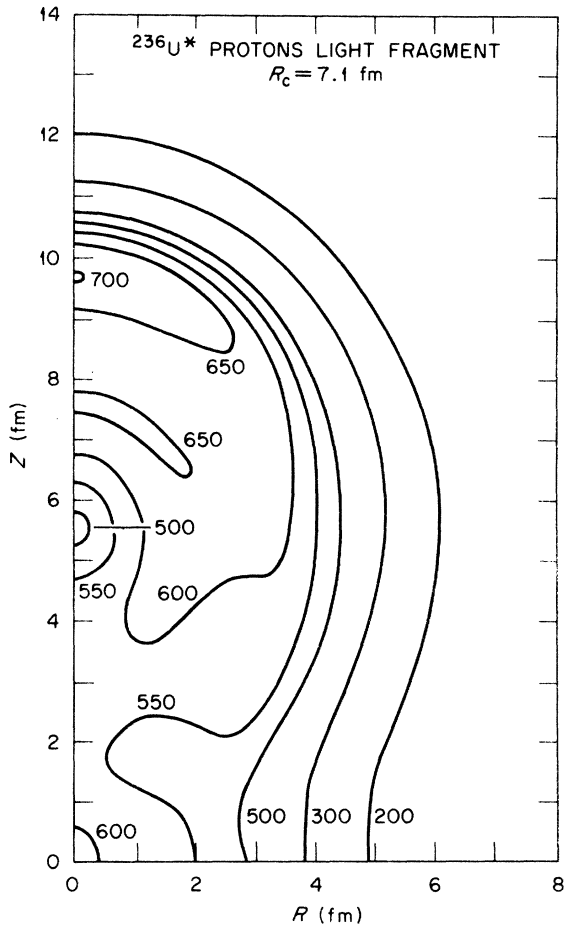

FIG. 6. Proton density contour of the light fragment near $r_c=7.1$ fm. The neutron one is similar and not shown here.

to raise the possibility that the three modes of excitation discussed here, e.g., angular (multipole mode), radial (bubble modes), and isotopic (giant $T=1$ dipole modes), are the main components of the experimentally observed 25 MeV average[17] internal excitation energy of the fragments in a fission event. Figure 9 shows the average observed mass ratio as a function of the internal energy of the fragment. It can be seen that the value 139/97 found here is consistent with an average internal excitation energy of 20 MeV. Again this suggests one should compare the total energy of actual ground states of the fragments with the total energy of the configurations at the time of scission.

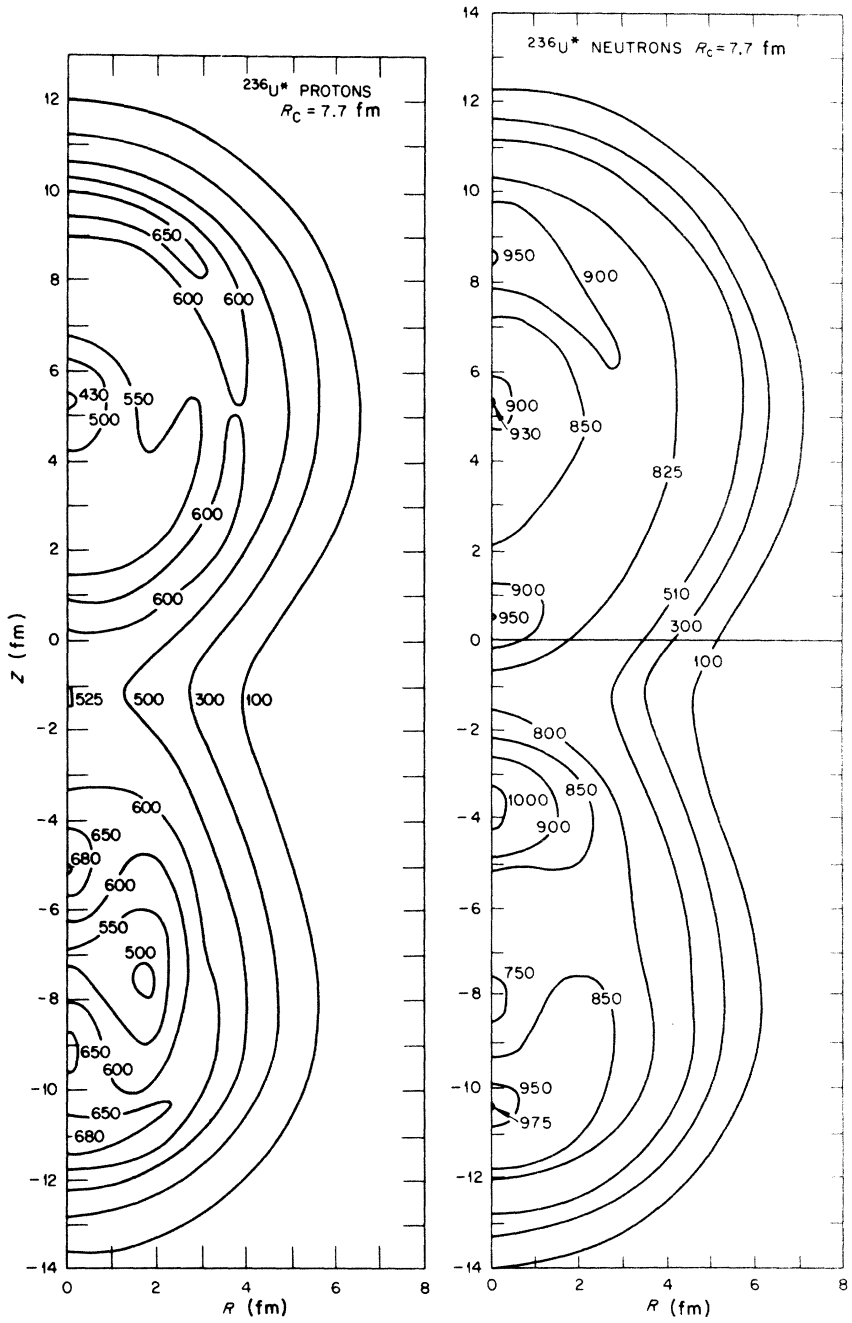

FIG. 7. (a) Proton density contours near $r_c = 7.7$ fm. The heavy fragment has absorbed most of the earlier ring structure and is already nearly spherical. The light fragment shows considerable quadrupole and octupole polarization. (b) Neutron density contours near $r_c = 7.7$ fm; see caption of (a).

Since this calculation is not immediate in our present approach, its results will be reported elsewhere.

The smoothness of the fission energy curve past the second barrier is to be contrasted with the prediction of the Nilsson-Strutinsky model.[18] However, we hasten to point out that only four points were compiled between the second barrier and the touching point due to the time-consuming nature of the present self-consistent constrained iterative

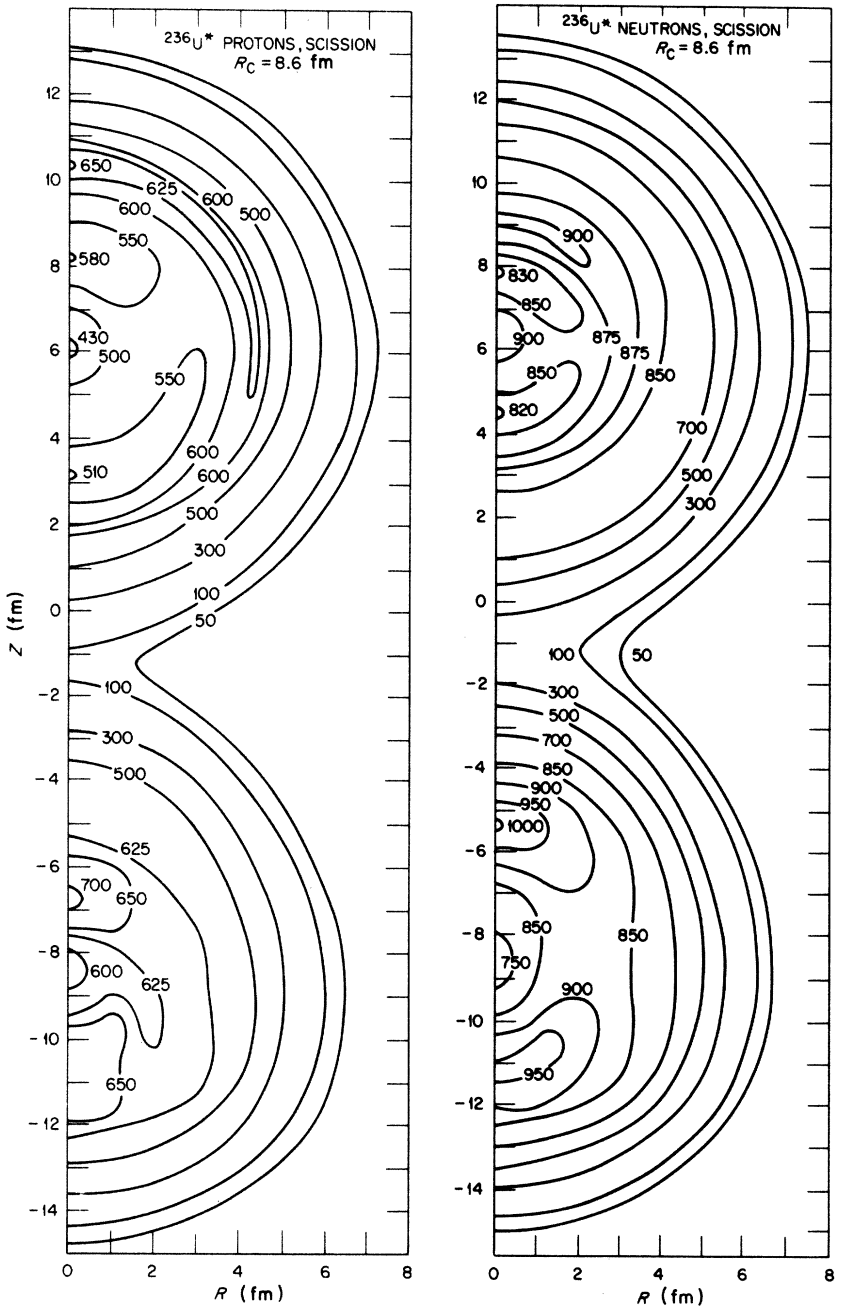

FIG. 8. (a) Proton density contours near scission. We have defined scission for convenience to be the point on the fission curve where the maximum density of the bridge in the neck region has been reduced to $\frac{1}{5}$ the average central density. The exact scission configuration is difficult to maintain because such a bridge tends to be unstable under our constrained iterations. The light fragment still retains a considerable quadrupole moment and some octupole moment. (b) Neutron density contours near scission. See (a) caption.

scheme (1 to 3 min/iteration). This, plus the fact that the shell correction energy depends on the assumed details of the pairing model invoked, may have prevented us from seeing other small fluctuations in the total binding energy. Of greater interest, however, is the possibility of a broad minimum due to the behavior of the liquid-Coulomb combined energies. As mentioned earlier, the existence of such a minimum may be predicated upon a delicate balance between surface Coulomb and bulk energies. Thus, parameter set I, which has the best over-all liquid drop properties, exhibits such a minimum, whereas it is not present for set III. Even though parameter set I is obviously superior over set III for heavy nuclei it is difficult to judge how good it really is. Therefore parameter set III may be used as a measure of how much the results can be affected, in particular around scission (touching point respectively) by different parameter choices. Comparing the results of sets I and III we conclude that there can be little doubt about the existence of a molecular cluster type minimum; its depth, however, is uncertain. It is interesting to note that our energy difference for barrier and minimum at the touching point of 14 to 24 MeV and the location at 14 and 12 fm, respectively, are close to non-self-consistent molecular cluster calculations by Noerenberg.[18] However, as long as the nuclear compressibility remains high and the symmetry energy cannot reliably be extracted, the effects of the Coulomb force and of the large value of N-Z cannot convincingly be extrapolated very far, although they appear to give correct results near the minimum and the second barrier.

As a matter of completeness we show in Fig. 10 the single-particle energy level diagrams for neutrons and protons as a function of β, the quadrupole deformation parameter of the density distribution. Scission occurs near $\beta = 1.2$; in that neighborhood the level spectrum was extrapolated further into the spherical configurations of the fragment shells. The position of the Fermi energy is indicated by the dotted lines. The gradual deepening of the Fermi sea is, of course, in agreement with the less pronounced effects of the symmetry and Coulomb energy as we approach the fragment shells. We also note that the Fermi sea lies in a region of relatively low level density immediately above the Fermi sea. This effect is, of course, related to the self-consistent nature of the present calculation; HF type models always tend to develop a gap immediately above the Fermi sea or failing that they often undergo yet another phase transition to a new deformed scheme where the gap can develop. Although the present level scheme shows many similarities with the Nilsson model level diagrams,[1] nearly as many discrepancies can be found. This is perhaps not too surprising once it is appreciated that the present level scheme not only leads to the correct shell-model correction energy, but also the correct liquid drop energies. As an illustration of this behavior, we note that the region near $\beta \cong 0.9$–1.0 shows near complete disorder in the level spectrum, in terms of shell effects. This is therefore the region where a Strutinsky average would be most accurate; e.g., a region of nearly exclusive liquid drop behavior. There one has the least well pronounced gap and the nuclear energy and motions during this period of increasing necking are as nearly collective as one can expect. Figure 7 near $r_c \cong 7.7$ fm shows the density in that liquid transition region. In particular, one notes that in Fig. 7 the octupole moment of the light fragment is such that the sharper end of the egg-shaped light fragment points inward as befits a fractioning drop, while in Figs. 3–5 the small octupole effects tend to make the joining edges flat (tips pointing outward) as was observed[7]

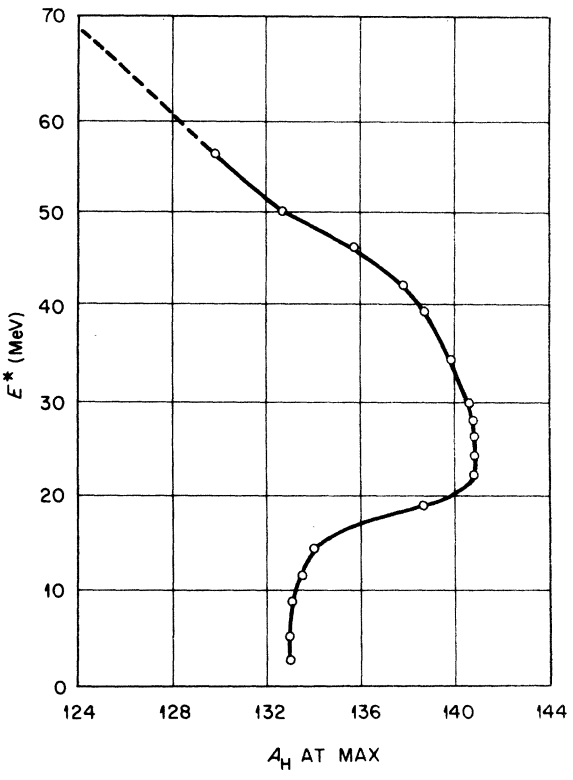

FIG. 9. Experimentally observed (Ref. 17) peak mass of the heavy fragment in the fission of ^{236}U, as a function of the total fragment internal excitation energy. The value $A_H \cong 139$ observed in the present calculation is consistent with an internal excitation of about 25 MeV.

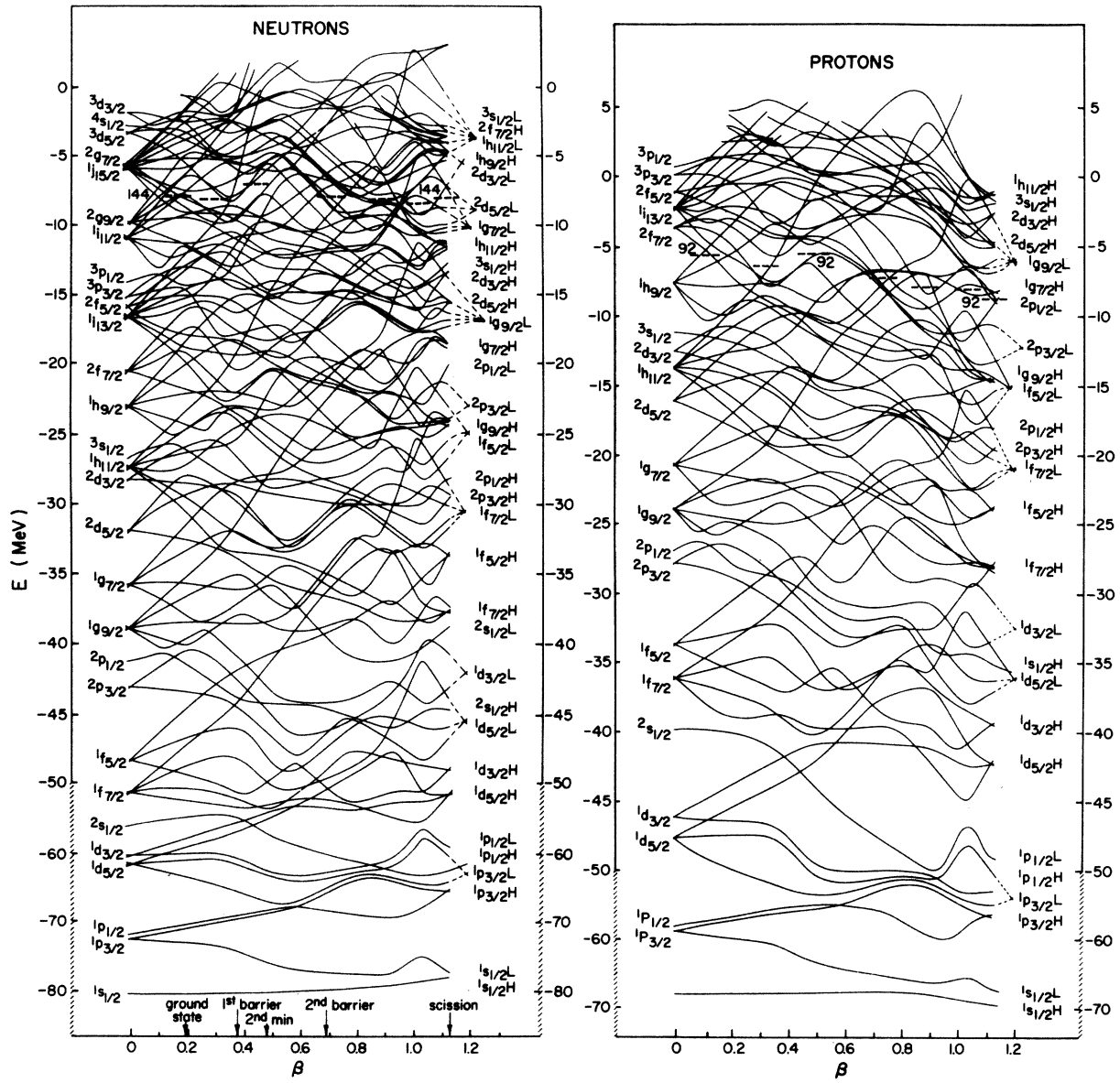

FIG. 10. (a) Neutron single-particle level diagram as a function of the mass distribution deformation parameter β, along the fission path of ^{236}U. See caption of Table IV for a definition of β. The vertical scale gives the approximate removal energy. The level displacements between the calculated values have been interpolated. Because of the asymmetry of the decay, the parity is good only for small values of β and once more for the extrapolated spherical fragment shells labeled L and H for the light and heavy fragments, respectively. The spherical shell identification quantum numbers are also given. (b) Proton single-particle level diagram as a function of the mass distribution deformation parameter. See caption of (a).

in the strongly shell correlated fission of the light nucleus $^{32}S \rightarrow {}^{16}O + {}^{16}O$.

To conclude this work we note that the present calculation shows the feasibility of realistic Brueckner-Hartree-Fock calculations for fission and fusion of heavy nuclei where the computed total energy includes both the shell model and the liquid drop contributions.

ACKNOWLEDGMENTS

We are grateful to H. W. Newson, L. C. Biedenharn, R. L. Becker, and C. Y. Wong for several stimulating discussions of the topics covered here. Our special thanks go to G. R. Satchler for continued support and encouragement throughout this work.

*Research jointly sponsored by the National Science Foundation and the Army Research Office (Durham), by the U. S. Atomic Energy Commission Contract No. AT(11-1)-3074, and by the U. S. Atomic Energy Commission under contract with Union Carbide Corporation.

†Guest Assignee from Duke University, Durham, North Carolina 27706, during the summer of 1973.

‡Consultant to Oak Ridge National Laboratory, Oak Ridge, Tennessee 37830 under contract with Oak Ridge Associated Universities.

§Present address: Environmental Systems Corp., P. O. Box 2525, Knoxville, Tennessee 37901.

[1]W. D. Myers and W. J. Swiatecki, Ann. Phys. (N.Y.) 55, 395 (1969); V. M. Strutinsky, Nucl. Phys. A95, 420 (1967); A122, 1 (1968); U. Mosel and H. W. Schmitt, *ibid.* A165, 73 (1971); U. Mosel, J. Maruhn, and W. Greiner, Phys. Lett. 34B, 587 (1971); M. G. Mustafa, U. Mosel, and H. W. Schmitt, Phys. Rev. C 7, 1519 (1973); M. G. Mustafa and H. W. Schmitt, *ibid.* 8, 1924 (1973).

[2]M. Bolsterli, E. O. Fiset, J. R. Nix, and J. L. Norton, Phys. Rev. C 5, 1052 (1972).

[3]M. Brack, J. Damgaard, A. S. Jensen, H. C. Pauli, V. M. Strutinsky, and C. Y. Wong, Rev. Mod. Phys. 44, 320 (1972).

[4]D. Vautherin and D. M. Brink, Phys. Rev. C 5, 626 (1972); H. Flocard, P. Quentin, A. K. Kerman, and D. Vautherin, Nucl. Phys. A203, 433 (1973); D. Vautherin, Phys. Rev. C 7, 301 (1973).

[5]K. A. Brueckner, J. L. Gammel, and H. Weitzner, Phys. Rev. 110, 431 (1958); K. A. Brueckner and D. T. Goldman, *ibid.* 116, 424 (1959); K. A. Brueckner, H. W. Meldner, and J. D. Peres, Phys. Rev. C 6, 773 (1973); H. A. Bethe, Phys. Rev. 167, 879 (1968); J. W. Negele and D. Vautherin, Phys. Rev. C 5, 1472 (1972).

[6]H. W. Meldner, Phys. Rev. 178, 1815 (1969); H. W. Meldner and C. M. Shakin, Phys. Rev. Lett. 23, 1302 (1969).

[7]D. Kolb, R. Y. Cusson, and M. Harvey, Nucl. Phys. A250, 1 (1973); D. Kolb, unpublished; R. Y. Cusson, D. Kolb, and H. P. Trivedi, Nuovo Cimento Lett. 7, 793 (1973).

[8]R. Y. Cusson, H. P. Trivedi, H. W. Meldner, and M. S. Weiss, unpublished.

[9]D. Kolb and R. Y. Cusson, Z. Phys. 253, 282 (1972).

[10]V. A. Chepurnov and P. E. Nemirovsky, Nucl. Phys. 49, 90 (1963).

[11]W. Bertozzi, J. Friar, J. Heisenberg, and J. W. Negele, Phys. Lett. 41B, 408 (1973).

[12]H. W. Newson, Phys. Rev. 122, 1224 (1961); Bull. Am. Phys. Soc. 17, 440 (1972).

[13]H. C. Lee and R. Y. Cusson, Ann. Phys. (N.Y.) 72, 353 (1972).

[14]J. Heisenberg *et al.*, in *Proceedings of the International Conference on Nuclear Physics, Munich, 1973,* edited by J. de Boer and H. J. Mang (North-Holland, Amsterdam/American Elsevier, New York, 1973).

[15]C. E. Bemis, Jr., F. K. McGowan, J. L. C. Ford, Jr., W. T. Milner, P. H. Stelson, and R. L. Robinson, Phys. Rev. C 8, 1466 (1973).

[16]C. Y. Wong and D. Kolb, unpublished.

[17]H. W. Schmitt, in *Proceedings of the Second International Symposium on Physics and Chemistry of Fission, Vienna, 1969* (International Atomic Energy Agency, Vienna, 1969), p. 67.

[18]S. Yamiji, S. Suekane, and K. Harada, in *Proceedings of the International Conference on Nuclear Physics, Munich, 1973,* edited by J. de Boer and H. J. Mang (see Ref. 14); W. Noerenberg, Phys. Lett. 31B, 621 (1970); Phys. Rev. C 5, 2020 (1972); P. Mueller and J. R. Nix, Los Alamos Scientific Laboratory Report No. LA/UR/73/1036, 1973 (unpublished); W. M. Howard and J. R. Nix, in Proceedings of the Third International Atomic Energy Symposium on the Physics and Chemistry of Fission, Rochester, 1973 (unpublished).